Energy and Angular Distributions of Particles Desorbed From Surfaces Using Multiphoton Resonance Ionization Detection

R. Maboudian, M. El-Maazawi, Z. Postawa, C. T. Reimann*, G. P. Malafsky*, D. Hrubowchak, M. Ervin, B. J. Garrison and N. Winograd

Penn State University, Department of Chemistry
152 Davey Laboratory, University Park, PA 16802

ABSTRACT

Multiphoton resonance excitation has been employed to ionize neutral atoms and molecules desorbed from surfaces bombarded by 5 keV Ar+ ion beams. By positioning a laser beam above the target it is possible to image the ions onto a microchannelplate detector and to obtain energy and angle-resolved distributions. These distributions may be compared directly to classical dynamics computer simulations of the ion/impact event. Results are presented using the {001}, {111} and {331} crystal faces of Rh to illustrate how the distributions contain specific structural information. Moreover, we compare the distributions from {111} to secondary ion angular distributions. This comparison suggests that there are special impact points which lead to ion formation from clean metal surfaces. Finally, we present preliminary measurements for the MPRI of pyrene molecules desorbed from polycrystalline gold surfaces. The results suggest this technique may be valuable for monitoring reaction intermediates present at very low concentration on catalyst surfaces.

1. INTRODUCTION

Energetic particle bombardment of solids and surfaces has become an important tool for their characterization and modification. With this approach, the kinetic energy of the primary particle, typically a few eV to a few thousand eV, exceeds the binding interactions normally present in chemical bonds. Because of this energy difference, a variety of novel and intriguing chain of events are rapidly set in motion subsequent to the impact event. Atoms may be significantly displaced from their equilibrium positions. Original chemical bonds may be broken with new ones formed. Energetic collisions may give rise to electronic excitation, ionization and desorption of atomic or molecular components of the bombarded solid.

These phenomena have led to important applications. A major impetus for research has been, of course, in the microelectronics area where ion implantation of dopant ions[1] and reactive ion etching of semi-conductors are hot topics.[2] There is also interest in evaluating surface processes which occur when energetic ions and molecules interact with non-linear optical materials.

Our research has been focused toward gaining a fundamental understanding of the ion/solid interaction event. On the theoretical side we have pursued the development of accurate models which can be used to either explain existing experimental results or to help in guiding the invention of completely new experimental approaches. Most recently, we have employed many-body force fields constructed using the embedded atom method (EAM).[3] From the experimental side, we have been particularly interested in angle-resolved desorption measurements of both ions and neutral atoms and molecules from single crystal targets. These measurements are extremely valuable in providing detailed experimental data for comparison to the theoretical calculations and as a check on their reliability. They have also been useful in elucidating the binding geometry of small atoms and molecules on surfaces. In 1982, we demonstrated that the neutral component could be effectively post-ionized using laser initiated multiphoton resonance excitation.[4]

In this paper, we illustrate how energy and angle-resolved neutral (EARN) data contain structurally specific information, also predicted using computer simulations. These data are presented for Rh{111}, Rh{331}, Rh{001} and for oxygen adsorbed in a p(2x2) overlayer on Rh{111}, all bombarded by 5 keV Ar+ ions. Moreover, we compare the EARN distribution to the secondary ion angular distribution for Rh{111}. This comparison suggests that there are special impact points which lead to ion formation from clean metal surfaces.

Current addresses: *Naval Research Laboratory, Washington, DC 20375

2. EXPERIMENTAL SETUP

The experimental apparatus has been described in detail elsewhere.[5] Briefly, the measurements are performed in a cryopumped ultra–high vacuum system with a base pressure of 2 x 10^{-10} Torr. The chamber is equipped with a LEED/Auger system and apparatus for sputter cleaning as well as laser–based detection of desorbed neutrals. Samples are mounted on a precision sample manipulator capable of vertical, horizontal, polar and azimuthal motions. The manipulator is equipped with an electron–beam heater for sample annealing; the temperature is monitored using a chromel–alumel thermocouple spot–welded to the sample holder. Rh single crystals were optically polished and oriented to ±0.5° using Laue back–reflection. The *in–situ* sample preparation for Rh{111} and Rh(331) were described previously. For Rh{100}, additional exposure to hydrogen at 1.0 x 10^{-7} Torr pressure and 330°C for 20 mins was performed.

The EARN distributions were measured in the following way. A 200–ns pulse of 5 keV Ar^+ ions, consisting of approximately 7.5 x 10^6 ions, was focused to a 2–mm spot on the sample. Upon impact of the ion beam, an ion extraction field is activated for the duration of the experiment to suppress the ejected secondary ions. A Nd:YAG pumped dye laser with a frequency doubler, operating at 312 nm, is employed to ionize the desorbed Rh atoms. The time delay between the ion–pulse impact and the ribbon–shaped laser pulse (~0.5 mJ by 6 nsec) determines the TOF, and in turn the kinetic energy, of the probed atoms. The ionized particles are then accelerated onto a multichannel plate detector and displayed on a phosphur screen. This signal is monitored by an image processing system (CoHU 6400 CCD video camera along with Data Translation DT–2651 frame grabber) and is stored on a MicroVAX Station II minicomputer for further deconvolution.

3. RESULTS AND DISCUSSION

3.1 Channeling and Blocking on Single Crystal Surfaces

It is of fundamental interest to accurately measure the trajectories of an atom in its ground electronic state desorbing from an ion bombarded single–crystal substrate and to compare these trajectories with those calculated using molecular dynamics computer simulations. These measurements have become possible in the last few years using the EARN technique and are extremely important for validating the reliability of any theory. The Rh{111} surface bombarded at normal incidence by 5 keV Ar^+ ions has served as a convenient model system for these studies.[7] The structure of this surface, as in Fig. 1, has been well–characterized

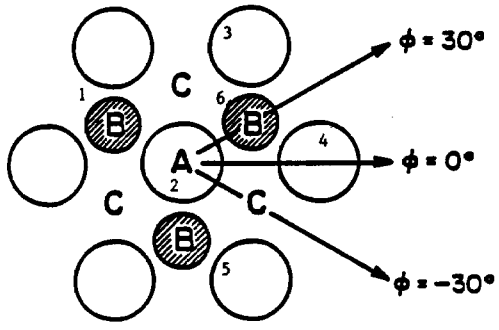

Figure 1. A polar angle of 0° is normal to the surface and 90° is grazing. Open circles designate first layer atoms and shaded circles second–layer atoms. The letters A, B, and C designate possible adsorption sides for oxygen atoms.

using LEED and is known to exhibit little surface relaxation or reconstruction. Note that for the {111} face of this face–centered–cubic lattice, the surface atoms exhibit six–fold symmetry. The 3 second–layer atoms, however, create bulk 3–fold symmetry with characteristic azimuthal directions along <111> ($\phi = 0°$ in our notation), <211>, $\phi = -30°$ and <112>, $\phi = +30°$. The experimental EARN distributions for this crystal face along $\phi = \pm 30°$ are shown in Fig. 2a. The measurements were recorded by bombardment at normal incidence with a series of 200 ns pulses of 5 keV Ar^+ ions (~2 x 10^6 ions/pulse). The desorbed Rh atoms were then ionized above the surface using the laser–based MPRI method described in section 2. It is important to note that these data were recorded with a total dose of less than 10^{11} Ar^+ ions/cm^2 so that the influence of surface damage is minimized.

It is possible to gain a great deal of mechanistic information from these trajectories by comparison to molecular dynamics calculations performed either using pair–potentials or using many–body (EAM) potentials. These sequences begin with the alignment of atomic motions inside the solid. As these motions cause ejection of first–layer atoms, further focusing is caused by channeling or blocking by other first–layer atoms. For example, the highest intensity is observed along the open crystallographic directions ($\phi =$

±30° in our case) and the minimum intensity is observed along the close–packed crystallographic direction ($\phi = 0°$). If only surface processes were important, the peaks at $\theta = -37°$, $\phi = -30°$ and $\theta = 42°$, $\phi = 30°$ should be equal in intensity and not unequal as shown in Fig. 2. The additional intensity at $\theta = -37°$, $\phi = -30°$ arises mainly from the ejection of atom 2 by atom 1 with

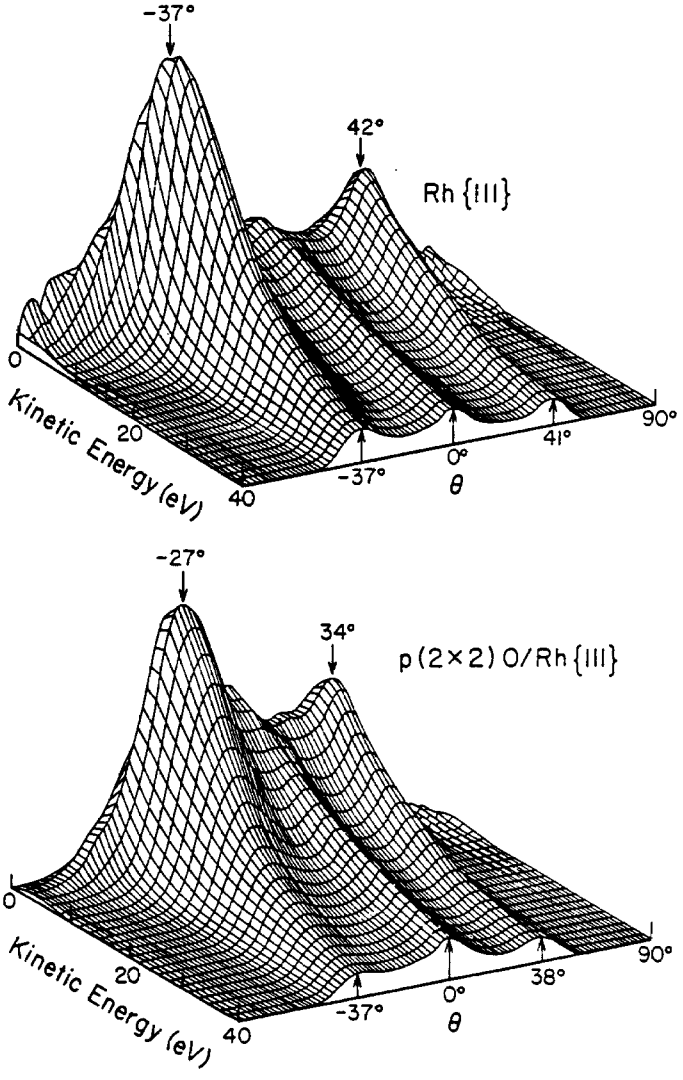

Figure 2. The EARN intensity maps for clean Rh{111} and p(2x2)O/Rh(111}. The plots are normalized to the highest intensity peak in both cases. The positive values of θ are recorded along $\phi = 30°$ and the negative values of θ are recorded along $\phi = -30°$ (from reference 7).

first–layer focusing by atoms 4 and 5. The peak at $\theta = 42°$ and $\phi = 30°$ is lower in intensity by a factor of 0.5 at low kinetic energy (KE) since no such mechanism is available along this azimuth. The peak at $\theta = 0°$ arises mainly from ejection of the second–layer atom 6 which is focused upward by atoms 2, 3 and 4. These curves may be accurately calculated using the EAM–molecular dynamics approach, a powerful testament to the validity of the channeling and blocking concepts.

A simple test of the consistency between experiment and theory is to examine other crystal faces of Rh and to look for similar channeling and blocking mechanisms. The Rh{331} surface[8] is an interesting surface since it is a stepped structure with a (111) terrace that is three atoms wide. Its atomic arrangement is shown in Fig. 3. The corresponding EARN data and EAM calculations are shown in Fig. 4. The most interesting features of the angular distribution plot are that the ejection is strongly peaked at $\theta = 15°$ along the $\phi = +90°$ azimuth, and that the desorption along other crystallographic directions is considerably reduced. Note that these features are well–reproduced by the EAM calculations. The parameters in the potential function were unchanged from those used in the Rh{111} calculation. This agreement is quite important to see since the excess electron density present at the step edge might have altered the trajectory of the departing Rh atoms. These calculations conclusively show that the peak at $\theta = 15°$ arises from the same channeling mechanism operative for {111}. This polar angle corresponds to the $\theta = 37°$ peak observed

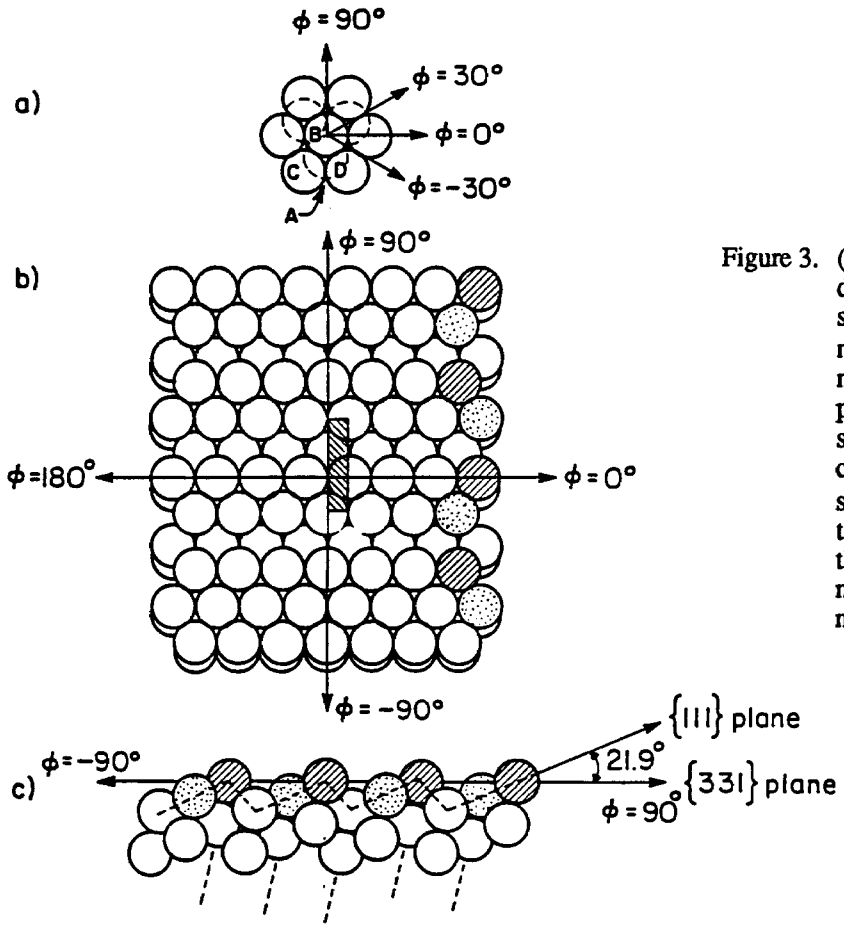

Figure 3. (a) Rh{111} surface indicating azimuthal directions used in the text. (b) Rh{331} surface indicating the definition of azimuths used in the text. The $\phi = 0°$ azimuth is the same as that in (a). The impact zone used in the classical dynamical simulation is shown at the center of the crystallite as a shaded box. (c) Rh{331} surface viewed from the $\phi = 0°$ direction. The shaded atoms correspond to the shaded atoms in (b). The dotted near–vertical lines indicate a major channeling direction (from reference 8).

from {111} except that the crystal orientation is simply tilted by 21.9° about $\phi = 0°$ as seen in Fig. 3. The reduced intensity along the other directions arises either from the presence of open channels in the crystal (near $\theta = 0°$) or from blocking due to the atomic step along $\phi = -90°$. Overall, the structure in the angular distributions is quite striking for both clean Rh{111} and Rh{331}, especially when compared to the simple $\cos^2\theta$ dependence exhibited by the polycrystalline Rh surface.

Similar anisotropies are observed for Rh atoms desorbed from the ion–bombarded Rh{001} surface. Both experimental and calculated polar angle distributions are shown in Fig. 5 for the open crystallographic direction, $\phi = 0°$, and the close–packed direction, $\phi = 45°$. The calculated curves were obtained with the same EAM potential employed for the Rh{111} and Rh{331} studies. Again, the overall agreement between the two cases is excellent.

A comparison between the polar angle distributions for Rh{111} and Rh{001} reveals additional details about the channeling and blocking mechanisms. Note that the peak in the polar angle distribution in the 10–20 eV range is larger for {001} ($\theta_{max} = 49°, \phi = 0°$) than for {111} ($\theta_{max} = 37°, \phi = -30°$). This difference arises since the open channel is larger on {001}, allowing more grazing take–off angles. The polar angle intensity maxima along the close–packed directions, however, are nearly identical for both crystal surfaces ($\theta_{max} = 34°$ for {001} and $\theta_{max} = 32°$ for {111}). This result is important since the distance to the nearest–neighbor atom along the close–packed direction is identical for both surfaces. Thus, the polar angle distributions are determined by the extremely local interactions experienced by the desorbing atom, and can be predicted from the presence or absence of channeling directions.

Since crystal structure via channeling and blocking strongly influences the EARN distributions, it follows that adsorbate atoms or molecules on single–crystal substrates should systematically alter the trajectories of the desorbing underlayer species.

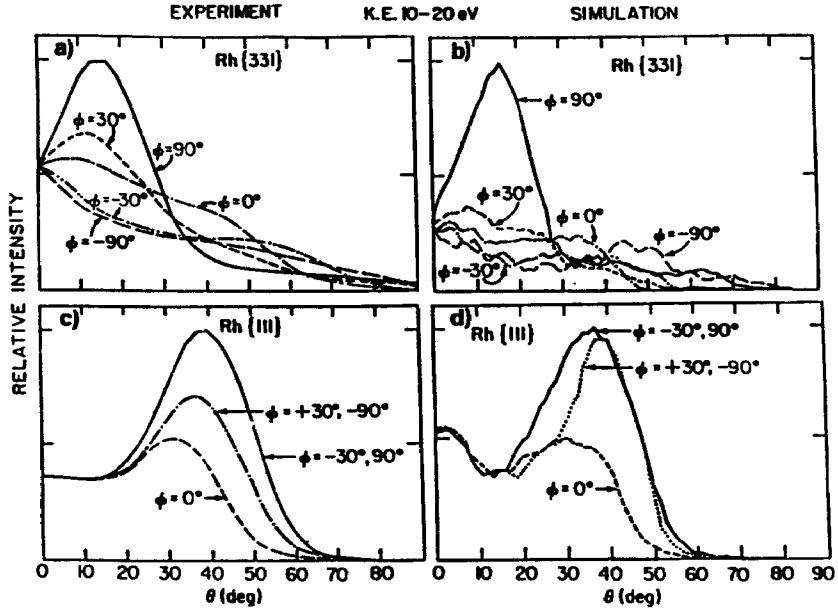

Figure 4. Polar angle Rh atom distributions of keV ion–induced desorption from Rh single crystals. The 10–20 eV kinetic energy range is shown. (a) Rh{331}, experimental data; (c) Rh{111}, experimental data; (b,d) calculated curves employing the EAM potential (from reference 8).

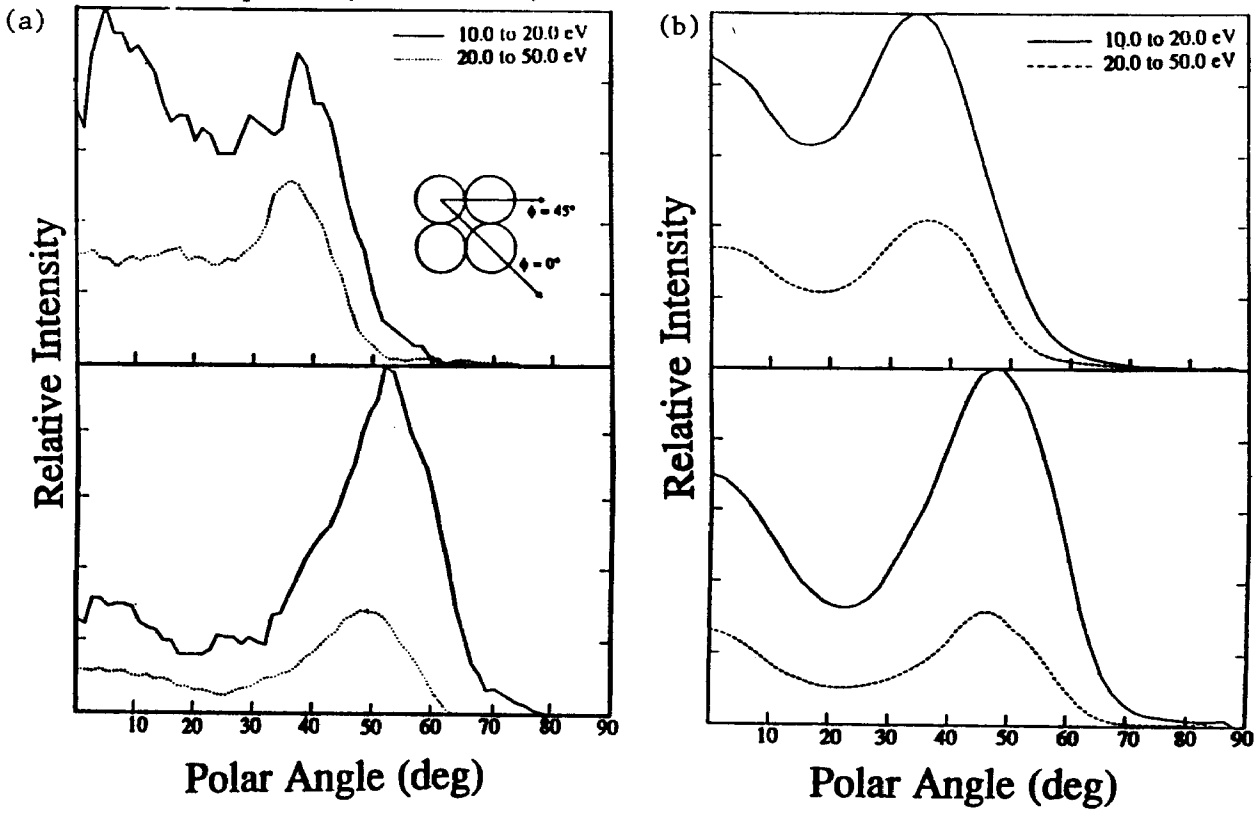

Figure 5. Polar angle distributions of Rh atoms desorbed from Rh{001}, in the azimuthal directions $\phi = 45°$ (top) and $\phi = 0°$ (bottom), for both, Simulation (a) and Experiment (b).

The concept has been tested in detail for the p(2x2) O ordered overlayer on Rh{111} with the EARN experiment.[9] For an atomic adsorbate of this sort, there are a number of possible high-symmetry binding sides including two different 3-fold hollow sites (often referred to as the B or hep site and the C or fcc site) and an on-top site (or A site). The simplest idea is that adsorption of oxygen atoms at a B site should preferentially block Rh atoms desorbing along the $\phi = +30°$ azimuth, adsorption at a C site should alternate Rh atoms leaving along $\phi = -30°$ while A site adsorption may have very little effect, except perhaps on the particles emitted at $\theta = 0°$. Preliminary polar angle measurements[7] as seen in Fig. 2b clearly show that the $\phi = -30°$ direction is preferentially reduced relative to either $\theta = 0$ or $\phi = +30°$ strongly suggesting C site adsorption.

These results are quite interesting since they clearly show how sensitive the desorption angular distributions are to small overlayer coverages. In this case, in addition to the observed perturbations in the EARN distributions, the total ground state neutral Rh atom yield was observed to decrease by a factor of about 2. These observations further illustrate that trajectory measurements which are to be compared with theory must be performed on well-cleaned and characterized surfaces and under low-dose conditions.

It would be gratifying to obtain the same excellent agreement between the p(2x2) O/Rh{111} EARN measurements and the EAM-molecular dynamics calculations as was found for the clean surface. The development of the EAM is not yet directly applicable, however, to chemisorbed overlayers such as oxygen. As an approximation, it has been possible to take a fairly rigorous look at overlayer effects by using EAM forces to describe the Rh-Rh interactions, but using pair-wise additive potentials to describe the Rh-O surface interactions. These simulations clearly confirm that the simple blocking ideas are correct, and yield EARN distributions for the Rh atoms that are in quite good agreement with experiment.[9]

Usually, kinetic energy distributions of ejecting atoms are not terribly relevant to studies involving surface structure. There is a situation associated with chemisorbed species, however, that merits closer attention. The KE distributions for clean Rh{111} and oxygen covered Rh{111} are shown in Fig. 6. Note that the peak in the KE spectra shifts by 2–5 eV to *lower* KE. The computer simulations suggest that this lowering arises from the fact that the underlying Rh atoms lose some energy as they escape through the overlayer oxygen atoms. The effect might be misinterpreted to mean that oxygen weakens the Rh surface binding energy since analytical models predict that the peak is proportional to 1/2 of this value.

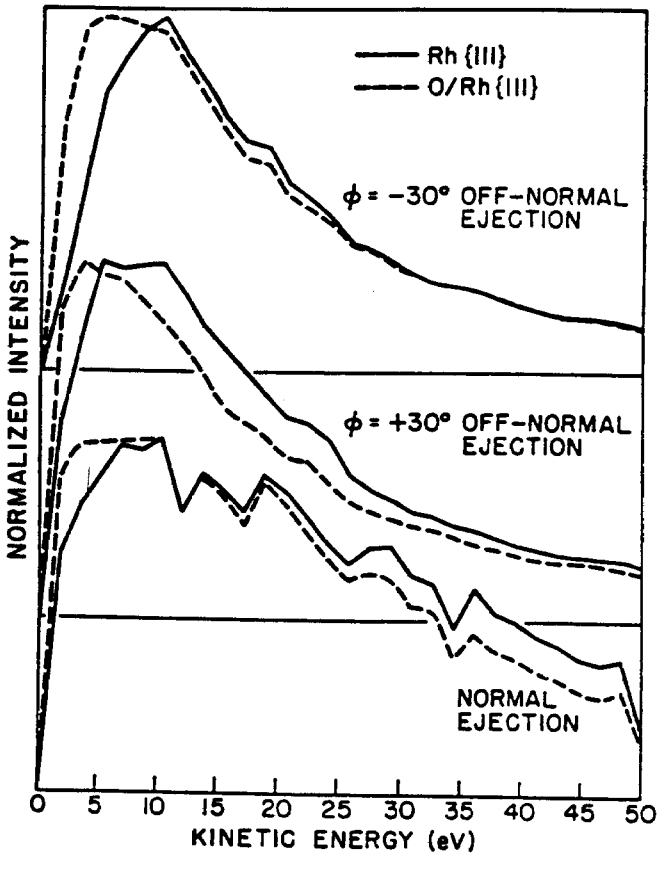

Figure 6. Experimental kinetic energy distributions of Rh atoms ejected from clean and oxygen-covered Rh{111}, taken at ejection angle $\theta = 45°$. p(2x2) LEED pattern was observed for the oxygen overlayer. The data are normalized to the same peak signal intensity. The polar angle resolution is ±3° (from reference 3).

3.2 Secondary Ion Fraction Measurements

The opportunity to measure EARN data is particularly valuable since it may be compared with similar data obtained for the ejection of Rh+ ions created during the ion impact event. This comparison of the ratio of secondary ions to neutral Rh atoms, R+, may be important for the development of theories for the secondary ionization process. Recently, Nourtier and coworkers[10] have presented a model in which the electronic structure of the solid is sufficiently distorted to shift the interaction of the ejecting particle with the substrate from the delocalized metal s–band to the more localized d–band. As a consequence of this perturbation, it is possible that excitations created in the collision cascade by a particular mechanism can survive to escape the surface. For clean metals where the value of R+ is inherently quite low, this effect may have a major influence on the ion distributions even though the corresponding neutral particle distribution may be unaffected. Molecular dynamics calculations of the ion–single crystal target that produce an anomolously high yield of particles.[11] This type of collision event has been discussed for many years[12] and has recently been termed a "megaevent".[11] At this point, it is unclear if there is a connection between Nourtier's proposal for the creation of localized states, "megaevents", and any observable property associated with R+.

The relevant kinetic energy distributions for Rh and Rh+ ions desorbed from Rh{111} are shown in Fig. 7. The curves were obtained using 3 keV Ar+ ion bombardment at normal incidence with detection at a polar angle, $\theta_d = 45°$. The most striking

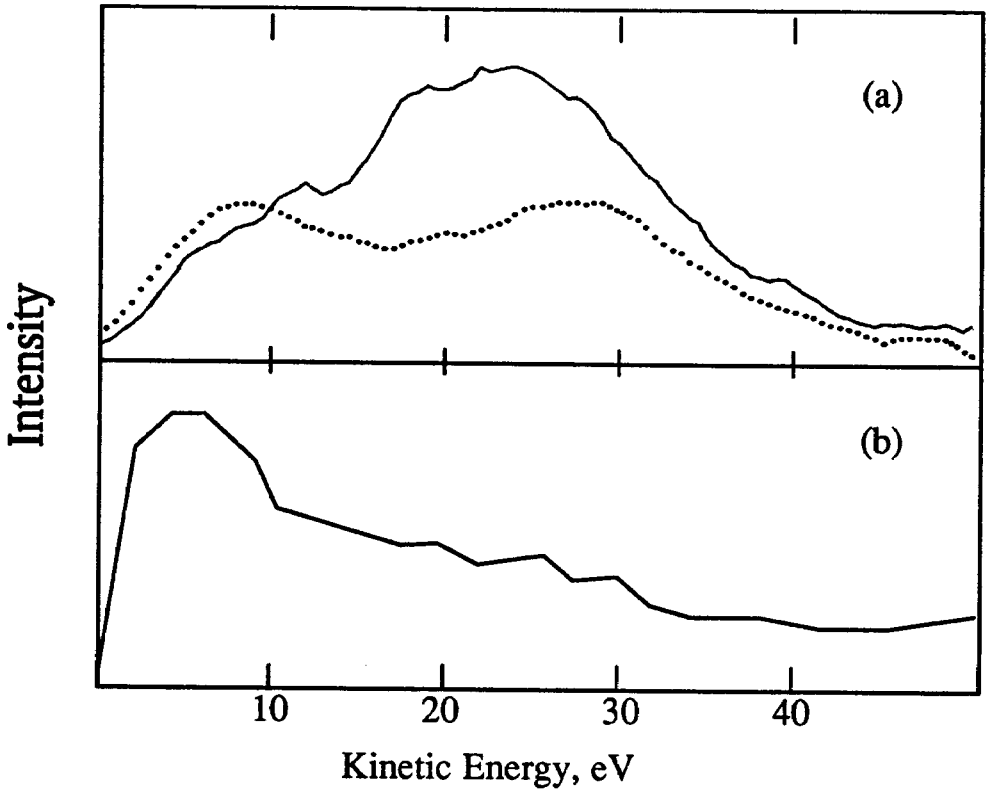

Figure 7. Kinetic energy distributions for Rh+ ions (a) and Rh neutral atoms (b) ejected from Rh{111} during bombardment at normal incidence by 3 keV Ar+ ions. In (a), the distributions are shown for the $\phi = +30°$ azimuth (solid line) and the $-30°$ azimuth (dotted line). In (b) the $+30°$ azimuth is shown. In all cases, the polar angle of detection is 45°.

feature of these results is the double peaked structure in the ion distributions which is not evident in the neutral atom distribution. The low energy peak occurs at 7–10 eV and the higher kinetic energy peak is seen at 22–28 eV. The relative intensity of the two peaks varies with the polar and azimuthal angles of detection. The high energy structure is most intense at $\theta_d = 45°$ at an azimuthal angle ϕ of $+30°$. As seen in the figure, this feature is reduced by about 50% for $\phi = -30°$. We also find that it steadily

diminishes in intensity with increasing polar angle for all azimuthal directions. We have not seen any evidence for this structure with the neutral distributions at any detection angle.

Preliminary molecular dynamics calculations provide an important clue to the origin of this structure. By analyzing the computed trajectories, we find that when second–layer atoms are ejected, they are accompanied by the ejection of several first–layer atoms. In fact, the yield of these processes can be 2 to 3 times as large as the average yield. This effect has also been noted for bombarded Cu crystals.[13] Moreover, these high yield collision sequences lead to ejection of atoms predominantly along the $\phi = +30°$ azimuth for a restricted energy range. The ratio of intensities for $\phi = +30°$ to $\phi = -30°$ is displayed in Fig. 2 for 3 different secondary particle kinetic energies. The yield minimum is defined as the minimum number of ejected particles per impact event that the collision sequence must produce in order to be counted. The enhanced yield for the 20 eV secondary Rh atoms relative to the other kinetic energy ranges is clearly evident in the figure.

3.3 Detection of Molecules Desorbed from Surfaces

It has been known for some time that ion beams can be used to desorb a wide variety of molecules from surfaces without significant fragmentation. A fraction of the molecules are ionized during desorption and may be detected using conventional mass spectrometry. Our group has been exploring the possibility of using MPRI to efficiently ionize neutral molecules after they have left the surface in order to improve on the SIMS experiment. The viability of this approach is not immediately obvious since molecular species possess a high density of states and the MPRI process can be quite complex. In earlier experiments, several groups have used laser desorption to inject nonvolatile molecules into supersonic jets of Ar atoms or CO_2 molecules.[14,15] This jet ensures that all the molecules will be in their ground states and that the spectroscopy will be well–defined. This approach yields elegant spectral quality but suffers in sensitivity. Another group has successfully employed MPRI to ionize molecules directly as they exit a capillary gas chromatographic (CGC) column.[16] These workers obtained excellent molecular ion signals on many molecules without using a supersonic jet expansion.

We have obtained preliminary data for the desorption of 5×10^{-12} moles of pyrene deposited onto a polycrystalline gold substrate. This molecule has an ionization potential of 7.42 eV and can be ionized with 2 photons of 280 nm. The results of these studies are shown in Fig 8(a) and (b). As seen in Fig 8a, using a peak power of 41 MW/cm^2, a strong pyrene molecular ion signal is seen with little fragmentation. Only a weak gold signal is observed presumably due to non–resonant excitations. When the laser beam is focused to obtain a power density of 5×10^9 W/cm^2, as seen in Fig. 8b, the molecular ion intensity is greatly reduced,

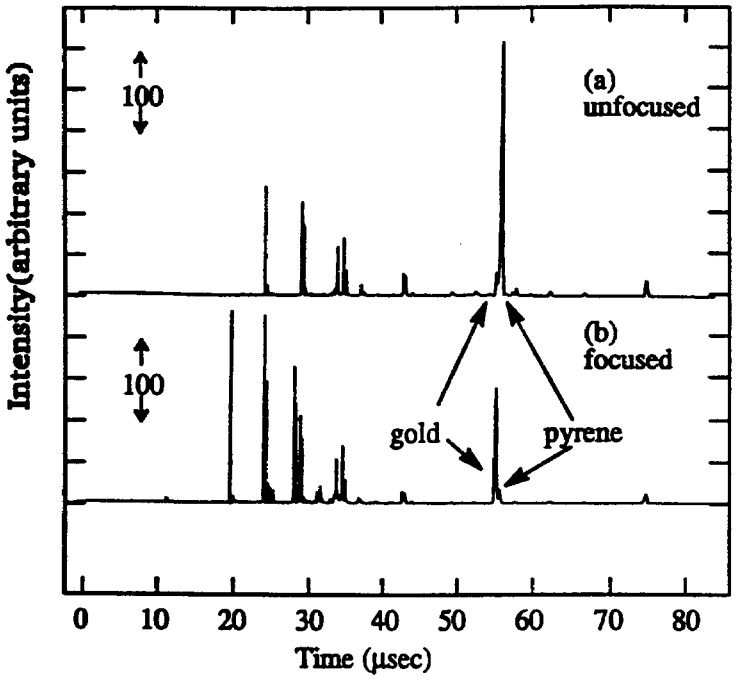

Figure 8. Time–of–flight MPRI spectrum of pyrene indicating the molecular ion at 202 amu for an (a) unfocused and a (b) tightly focused laser beam. The TOF–SIMS spectrum using a 510 ns Ar+ ion pulse is shown in (c). The time scale is somewhat arbitrary. The ion pulse occurs at ~3 μs, and the laser is activated after 9 μsec. Masses are then computed from known elements.

fragmentation is higher, and the non–resonant gold signal dominates the spectrum. These results are quite encouraging and suggest that the MPRI method may become a powerful detection scheme for a variety of surface chemistry experiments.

4. Acknowledgement

The authors greatfully acknowledge the financial support of the National Science Foundation, the Office of Naval Research and the IBM Corporation for the support of this work. Penn State University supplied a generous grant of computer time for the computer simulations. B.J.G. thanks the Camille and Henry Dreyfus Foundation for a Teacher–Scholar Award.

5. References

1. Ion Implantation, Science and Technology, Academic Press, Boston, 1988.
2. H. F. Winters and J. W. Coburn, *J. Vac. Sci. Tech.* B3, 1376 1985.
3. B. J. Garrison, N. Winograd, D. M. Deaven, C. T. Reimann, D. Y. Lo, T. A. Tombrello, and M. H. Shapiro, *Phys. Rev.* B37, 7197 (1988)
4. N. Winograd, J. P. Baxter and F. M. Kimock, *Chem. Phys. Lett.* 88, 581 1982.
5. P. H. Kobrin, G. A. Schick, J. P. Baxter and N. Winograd, *Rev. Sci. Instrum.* 51, 1354 1986.
6. L. A. DeLouise and N. Winograd, *Surface Sci.* 138, 417 1984.
7. N. Winograd, P. H. Kobrin, G. A. Schick, J. Singh, J. P. Baxter and B. J. Garison, *Surf. Sci. Lett.* 176, L817 1986.
8. C. T. Reimann, K. Walzl, M. El–Maazawi, D. M. Deaven, B. J. Garrison and N. Winograd, *J. Chem. Phys.* 89, 2539 1988.
9. C. T. Reimann, M. El–Maazawi, K. Walzl, B. J. Garrison and N. Winograd, *J. Chem. Phys.* 90(3), 2027 1989.
10. A. Nortier, J. P. Jardin and J. Quazza, *Phys. Rev.* B37, 10628 1988.
11. D. E. Harrison, Jr. *CRC Review in Solid State Materials Science* 14, S1 1988.
12. P. Williams, *Surf. Sci.* 90, 588 1979.
13. M. H. Shapiro, P. K. Haff, T. A. Tombrello, D. E. Harrison, Jr. and R. B. Webb, *Rad. Eff.* 89, 234 1985.
14. J. Grotemeyer, U. Boesl, K. Walter and E. W. Schlag, *Org. Mass Spectrom.* 21, 645 1986.
15. D. M. Lubman and R. Tembreull, *Anal. Instrum.* 16, 117 1987.
16. R. L. M. Dobson, A. P. D'Silva, S. J. Weeks and V. A. Fassel, *Anal. Chem.* 58, 2129 1986.